

Characterization of carrier-envelope phase-sensitive photocurrent injection in a semiconductor

Peter A. Roos, Xiaoqin Li, Jessica A. Pipis, Tara M. Fortier, and Steven T. Cundiff

JILA, National Institute of Standards and Technology and the University of Colorado, Boulder, Colorado 80309

Ravi D. R. Bhat and John E. Sipe

Department of Physics, University of Toronto, Toronto, Ontario M5S 1A7, Canada

Received July 16, 2004; revised manuscript received August 18, 2004; accepted August 24, 2004

We characterize the manner in which the carrier-envelope phase of ultrashort pulses can control quantum interference of injected photocurrents in low-temperature-grown gallium arsenide. We verify the predicted linear and square-root dependences of the generated current on the average optical powers of the low (ν) and high (2ν) frequency wings of a pulse spectrum, respectively. When scanning the time delay between these two colors, the signal amplitude exhibits a temporal width of 72 fs. The generated signal behaves as an ideal current source for loads below ~ 100 k Ω . This behavior allows us to increase the signal detection bandwidth from 25 kHz with a voltage amplifier to 830 kHz by use of a transimpedance amplifier; higher bandwidths are possible. We discuss how transimpedance amplification could also enable the quantum-interference photocurrent signal to be measured by use of materials with longer carrier lifetimes, such as intrinsic GaAs. © 2005 Optical Society of America

OCIS codes: 120.5050, 190.5970, 320.7100.

1. INTRODUCTION

The advent of ultrafast mode-locked lasers has enabled the generation of highly repetitive optical pulse trains with pulse durations that are comparable to the optical carrier period. For such few-cycle pulses, a variety of physical processes become sensitive to the phase of the carrier wave relative to the peak of the pulse envelope (carrier-envelope phase ϕ_{CE}).¹ Without active stabilization, ϕ_{CE} wanders uncontrolled from one pulse to the next because of fluctuations in the difference between the group and the phase velocities within the mode-locked laser cavity.¹ Researchers have actively stabilized the time evolution of ϕ_{CE} so that it changes from pulse to pulse in a controlled manner and at a prescribed frequency called the carrier-envelope offset frequency (f_0).²⁻⁴

The most common technique currently used to stabilize f_0 is ν -to- 2ν self-referencing.³⁻⁵ This technique involves frequency doubling the low-frequency wing (ν) of the pulse spectrum and optically mixing it with the high-frequency wing (2ν) of the pulse spectrum. The resulting rf beat note between these two optical fields relative to a stable oscillator is used as feedback in a phase-locked loop to stabilize f_0 of the laser. This method requires a pulse spectrum that spans a factor of 2 in frequency (an octave-spanning spectrum). Although octave spectra have recently been generated directly from Ti:sapphire oscillators,^{6,7} spectral broadening in nonlinear optical fiber is typically required to generate sufficient light at the two harmonic frequencies.⁸

The immediate effect of stabilizing f_0 was realized in the frequency domain where the spectral composition of the stabilized pulse train can be used to link microwave

and optical frequency standards and to provide stable optical frequency references.⁹⁻¹² More recently, f_0 stabilization has assisted in investigating physical processes that are sensitive to ϕ_{CE} . With amplified pulses, Paulus *et al.* showed that the direction of emitted photoelectrons from photoionized krypton gas can depend on ϕ_{CE} .¹³ When using phase-stabilized pulses, the researchers were able to use this above-threshold ionization technique to reproducibly measure and control ϕ_{CE} itself, rather than just its evolution.¹⁴ This achievement represented a significant step in the characterization of optical pulses and also led to the first direct observation of the Gouy effect on the carrier-envelope phase.¹⁵ In related work, researchers have shown that coherent soft-x-ray (high harmonic) generation from amplified pulses that is due to the ionization of gases can also display ϕ_{CE} dependence.^{16,17} Using unamplified but shorter duration pulses, Apolonski *et al.* and Dombi *et al.* investigated the sensitivity of multiphoton-induced photoelectron emission from gold surfaces to ϕ_{CE} .^{18,19} With improved signal strength, this solid-state measurement technique appears attractive for direct measurement and stabilization of ϕ_{CE} itself.

Processes in semiconductors that are sensitive to ϕ_{CE} have also been investigated. Researchers have predicted and recently observed sensitivity in GaAs to ϕ_{CE} that is due to interference between Rabi sidebands in the carrier-wave Rabi flopping regime.²⁰⁻²³ Mücke *et al.* also showed that the spectral broadening and second harmonic generation required to generate a heterodyne beat note by means of the standard ν -to- 2ν technique can be performed within a single ZnO crystal.²⁴ More recently, the same group attained sufficient signal strength from

this ZnO system to stabilize f_0 .²⁵ This achievement appears promising for simplification of the stabilization apparatus.

Here we characterize a quantum-interference process in semiconductors that is sensitive to ϕ_{CE} of ultrashort pulses. Illumination of a direct-gap semiconductor ordinarily generates little or no net current because absorption of photons occurs symmetrically in momentum space. In other words, carriers are generated with equal probability in any two opposite directions, resulting in no net carrier flow. However, theoretical and experimental studies have shown that quantum interference between one- and two-photon absorption can disrupt this symmetry and lead to a net current.^{26–29} The relative phase of the light fields that drive the one- and two-photon processes dictates the direction and magnitude of the resulting current. Contrary to most discrete-level atomic systems, both one- and two-photon transitions are allowed between the same initial and final states in a semiconductor because the Bloch states are not eigenstates of parity.

The asymmetry in the momentum-space carrier distribution arises from the fact that the two-photon transition probability from the valence to the conduction band is odd in momentum, and the single-photon transition probability is even. The overall carrier-generation probability is given by the modulus squared of the sum of these two transition probabilities, which yields an interference cross term that is odd in momentum. Therefore, when the relative phase of the light fields causes destructive interference for negative momentum, it causes constructive interference for positive momentum. The resulting momentum-space carrier imbalance produces a measurable current.

As illustrated conceptually in Fig. 1, this quantum-interference control (QIC) effect has been studied using two harmonically related pulse trains to drive the one- and two-photon processes in low-temperature-grown gallium arsenide (LT-GaAs).^{26–29} More recently the effect was predicted and observed to be sensitive to ϕ_{CE} of a single-pulse train in the same material.^{30,31} As can be seen in Fig. 1, this sensitivity occurs because the one- and two-photon absorption pathways can be established by the spectral wings of a single octave-spanning pulse. Here, we provide an experimental analysis of the single-

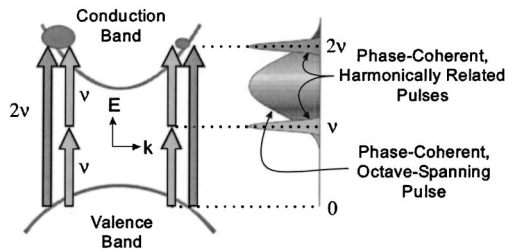


Fig. 1. Conceptual schematic showing quantum interference between one- and two-photon absorption in a direct-gap semiconductor. The two interfering absorption pathways can be driven by two harmonically related pulses or by the spectral wings of a single octave-spanning pulse. The interference can cause an imbalance in the otherwise symmetric carrier-population distribution in momentum space (represented by ovals), resulting in a net flow of carriers. The direction and magnitude of the resulting photocurrent are sensitive to the carrier-envelope phase for the single-pulse case.

pulse QIC phenomenon in LT-GaAs. We extend existing theoretical work for comparison with our measurements.

A number of related coherent control experiments that involve quantum interference between one- and two-photon absorption pathways in semiconductors, as well as in atomic and molecular systems, have been explored by use of harmonically related pairs of pulse trains. For example, quantum interference has been used to control spin currents in semiconductors, photodissociation in the HD^+ molecule, and photoelectron yield in both atoms and molecules.^{29,32–38} These processes should also be sensitive to the carrier-envelope phase of octave-spanning pulses.

2. THEORY

We consider an ultrashort pulse incident on a direct-gap semiconductor between two metal electrodes (for current collection). In the time domain, the complex electric field of the pulse, whose polarization direction is across the electrodes, is described by

$$E(t) = E_0(t)\exp[-i(2\pi\nu_C t + \phi_{CE})], \quad (1)$$

where $E_0(t)$ is the pulse envelope function, ν_C is the carrier frequency, and ϕ_{CE} is the carrier-envelope phase.¹ We assume that the spectral content of this pulse is sufficiently broad to excite both one- and two-photon absorption in the semiconductor, as shown in Fig. 1. In the frequency domain, the pulse is described by

$$\begin{aligned} \hat{E}(\nu) &= [\hat{E}_0(\nu) \otimes \delta(\nu - \nu_C)]\exp(-i\phi_{CE}) \\ &= \hat{E}_0(\nu - \nu_C)\exp(-i\phi_{CE}) \\ &= [\hat{E}_\nu(\nu) + \hat{E}_{2\nu}(\nu)]\exp(-i\phi_{CE}), \end{aligned} \quad (2)$$

where $\hat{E}_0(\nu)$ is the Fourier transform of $E_0(t)$. We split the original pulse spectrum $[\hat{E}_0(\nu - \nu_C)]$ into the portions below $[\hat{E}_\nu(\nu) = \hat{E}_0(\nu - \nu_C)\theta(\nu_C - \nu)]$ and above $[\hat{E}_{2\nu}(\nu) = \hat{E}_0(\nu - \nu_C)\theta(\nu - \nu_C)]$ the carrier frequency, where $\theta(x)$ is the Heaviside step function.³⁹ We designate $E_\nu(t)$ and $E_{2\nu}(t)$ to represent the time-domain envelopes of these two spectral portions of the pulse. In the experiment, we have the ability to adjust the optical power and time delay of the two spectral regions independently. Equation (2) shows that ϕ_{CE} is common to all frequency components of the pulse.

To model the quantum-interference effect that occurs in a semiconductor that is due to this pulse, we draw from and extend previous theoretical work based on two-pulse QIC experiments, where two distinct but coherently related pulses at frequencies ν and 2ν are focused onto a semiconductor.²⁸ First, we rewrite Eq. (3) from Ref. 28 with slightly altered notation:

$$\dot{J}(t) = 2\eta_C E_\nu^2(t - t_d)E_{2\nu}(t)\sin(2\phi_\nu - \phi_{2\nu}) - J(t)/\tau_C, \quad (3)$$

where $J(t)$ is the net photocurrent density generated. The field components $E_\nu(t)$ and $E_{2\nu}(t)$ have phases given by ϕ_ν and $\phi_{2\nu}$, respectively. The phenomenological current relaxation time τ_C is due to carrier momentum relaxation (~ 200 fs). The factor η_C differs from $|\langle \eta_{e,h} \rangle_{xxx}|$ in

Ref. 28 because we do not assume monochromatic illumination at ν and 2ν . Calculation of η_C for extended spectra is complicated and requires numerous integrals over frequency to account for such concerns as the frequency dependence of the current-injection tensor element and the spectral overlap of all the different frequency combinations that can contribute to the generated photocurrent (not just ν and 2ν).⁴⁰ We therefore defer calculation of η_C to a future publication. We neglect chirp despite the fact that it is present. We also neglect imperfect spatial overlap despite the fact that the spectral wings of our pulses exhibit similar spot sizes rather than the desired similar confocal parameters. We are concerned with comparing the qualitative behavior of a circuit model that involves the solution to Eq. (3) with the qualitative behavior of our experiment.

To facilitate solving Eq. (3), we first assume that the pulse durations of the contributing electric-field components at ν and 2ν are short compared to τ_C . This assumption is based on experimental measurements that we present in Section 4. When solving Eq. (3), this assumption allows us to neglect current decay during the pulse duration, yielding

$$J(t) = 2^{5/2} \eta_C (\mu_0 / \epsilon_0)^{3/4} n_\nu n_{2\nu}^{1/2} I_\nu I_{2\nu}^{1/2} \eta_T(t_d) \times \sin(2\phi_\nu - \phi_{2\nu}) \exp(-t/\tau_C), \quad (4)$$

where the pulses arrive at $t = 0$ for no delay, n_ν and $n_{2\nu}$ are refractive indices (assumed constant over the spectral regions that contribute to QIC), and I_ν and $I_{2\nu}$ are the peak irradiances of the two spectral components in the semiconductor (averaged over the absorption depth). The unitless temporal overlap integral,

$$\eta_T(t_d) = \frac{\int_{-\infty}^{\infty} |E_\nu(t - t_d)|^2 |E_{2\nu}(t)| dt}{\int_{-\infty}^{\infty} |E_\nu(t)|^2 |E_{2\nu}(t)| dt}, \quad (5)$$

accounts for different arrival times of the two contributing spectral components of the pulse.

We now consider the effect of a repetitive train of optical pulses that results in a repetitive train of current pulses. First, because the current decays rapidly compared with the temporal pulse separation T , we assume that the current generated by one pulse does not contribute to the next. Furthermore, the detection bandwidth for the metal-semiconductor-metal (MSM) structure and the measurement device is low compared with the pulse repetition rate. Our measurement is therefore sensitive only to the integrated (average) current generated, and we were not able to resolve the separation between individual pulses temporally. With these assumptions, Eq. (4) becomes

$$\langle J(t) \rangle = 2^{5/2} \eta_C (\mu_0 / \epsilon_0)^{3/4} n_\nu n_{2\nu}^{1/2} I_\nu I_{2\nu}^{1/2} \eta_T(t_d) \times \sin(2\phi_\nu - \phi_{2\nu}) \tau_C / T. \quad (6)$$

We retain the time dependence of the current density in Eq. (6) because the argument of the sine can vary slowly in time compared with all other characteristic times in the experiment. Specifically, Eq. (2) shows that ϕ_{CE} is

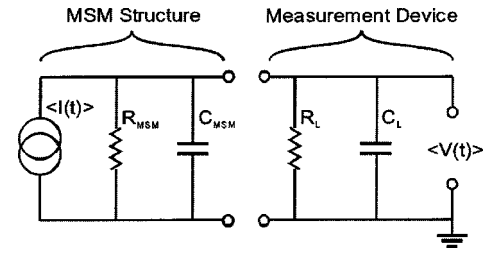


Fig. 2. Circuit diagram used to model the behavior of the QIC signal. The diagram shows the effective components of the MSM structure and the measurement device.

common to all frequency components of the pulse, therefore $\phi_\nu = \phi_{2\nu} = \phi_{CE}$. Thus the sensitivity of the QIC current to the carrier-envelope phase is evident in Eq. (6). However, without active stabilization, ϕ_{CE} wanders uncontrolled from pulse to pulse because of perturbations within the laser cavity. We assume that the time evolution of ϕ_{CE} is actively stabilized to a constant frequency such that¹

$$\phi_{CE}(t) = 2\pi f_0 t + \phi_0, \quad (7)$$

where ϕ_0 is an arbitrary phase offset and f_0 is the carrier-envelope offset frequency. This condition is routinely achieved in the laboratory.

Now, using $\langle I(t) \rangle = \langle J(t) \rangle S$, where S is the cross-sectional area of the current flow,²⁸ the effective average photocurrent generated is given by

$$\langle I(t) \rangle = I_0 \sin(2\pi f_0 t + \phi_0), \quad (8)$$

where

$$I_0 = 2^{5/2} \eta_C (\mu_0 / \epsilon_0)^{3/4} n_\nu n_{2\nu}^{1/2} I_\nu I_{2\nu}^{1/2} \eta_T(t_d) S \tau_C / T. \quad (9)$$

We use Eq. (8) as the current source in the circuit shown in Fig. 2, which differs in appearance from that given in Ref. 28. The only physical difference between the two circuits is that here the illuminated resistance measured across the MSM structure, or R_{MSM} , always remains large relative to the load resistance (R_L). This allows us to neglect the time and irradiance dependence of R_{MSM} . The capacitance of the MSM structure is given by C_{MSM} , whereas that of the load is given by C_L .

The signal we measure, $\langle V(t) \rangle$, is an oscillating voltage at frequency f_0 that is due to the oscillating current source. Using the circuit shown in Fig. 2, we solve for the measured voltage amplitude at that frequency, which yields

$$\langle V(f_0) \rangle = I_0 R [1 + (2\pi f_0 R C)^2]^{-1/2}, \quad (10)$$

where $R = (1/R_{MSM} + 1/R_L)^{-1}$ and $C = C_{MSM} + C_L$ are the total resistance and capacitance of the combined circuit, respectively. In the experiment, we either measured the oscillating voltage amplitude $I_0 R$ and its phase ϕ_0 by lock-in detection at f_0 or observed just the amplitude on a rf spectrum analyzer.

3. APPARATUS

The experimental setup used for these single-pulse QIC studies is shown in Fig. 3. We used a train of ~ 10 -fs pulses from a mode-locked Ti:sapphire laser with a repetition rate of 93 MHz, a center wavelength near 840 nm,

and an average power of 400–500 mW. The light from this laser was split into two portions: one for f_0 stabilization by use of a standard ν -to- 2ν interferometer^{3,4} and one for measurement of the QIC signal at f_0 . We spectrally broadened both portions in 4-cm lengths of microstructure optical fiber⁸ to produce sufficient light at the harmonically related optical frequencies ν (1064 nm) and 2ν (532 nm). We sent the first portion to a ν -to- 2ν interferometer, where we detected and phase locked f_0 to the frequency of a stable rf synthesizer.

With f_0 of the laser stabilized, we directed the second portion of light through a prism pair to spread the optical spectrum spatially. We reflected this dispersed light off two separate mirrors to make it possible to adjust the temporal delay between the ν and the 2ν spectral components. We then focused the light ($\sim 10\text{-}\mu\text{m}$ beam diameter for each color) onto the LT-GaAs sample in the semiconductor region between two gold electrodes separated by $30\ \mu\text{m}$. As in the two-pulse QIC studies, we used LT-GaAs to reduce the carrier lifetime to ~ 500 fs, thereby minimizing the current shunting effect of R_{MSM} during illumination.²⁸ Details of the sample and electrode structure are given in Ref. 30. We amplified the signal and utilized lock-in detection at the stabilized offset frequency f_0 . We also observed the beat note at f_0 on a rf spectrum analyzer. Using this setup, we explored the

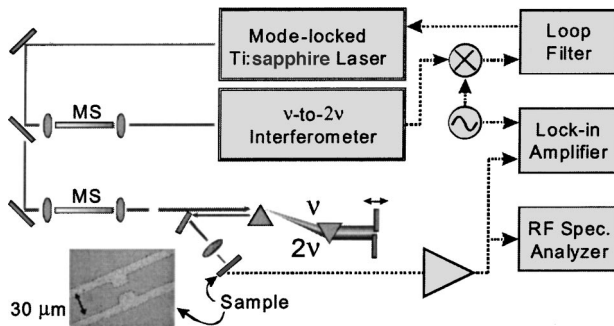


Fig. 3. Experimental setup used for single-pulse QIC studies. The ν -to- 2ν interferometer was used to stabilize f_0 by use of a feedback loop. A prism pair and split mirror were used to adjust the time delay between the light at frequencies ν and 2ν . The light was focused onto a $30\text{-}\mu\text{m}$ semiconductor gap between two metal strip-line electrodes. MS, microstructure fiber.

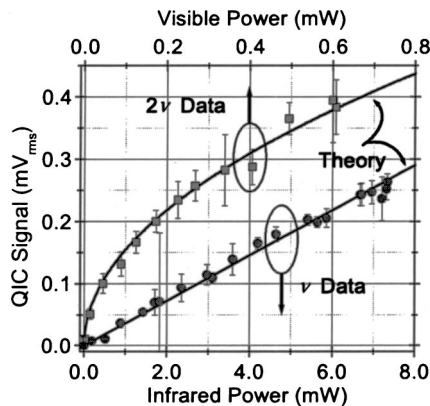


Fig. 4. QIC signal amplitude as a function of the average optical power at frequencies ν (circles) and 2ν (squares). The solid curves represent fits to the linear and square-root dependences that were predicted in Section 2.

dependence of the measured QIC signal amplitude on average optical power, temporal overlap, load impedance, and stabilization frequency.

4. RESULTS

A. Optical Power

A previous publication demonstrated the sensitivity of the semiconductor to static shifts in ϕ_{CE} .³¹ To substantiate the claim that this phase dependence is due to the QIC process, we first studied how the QIC signal amplitude depends on the average optical powers at frequencies ν and 2ν . We inserted a rotary variable attenuator into one color at a time directly before the split mirror shown in Fig. 3. Figure 4 shows the QIC signal amplitude measured on the lock-in amplifier as a function of the infrared (1064 nm, bottom axis, circles) and visible (532 nm, top axis, squares) average optical power. The error bars represent the standard deviation from ten measurements taken at each power level. The solid curves represent fits to linear and square-root behavior for frequencies ν and 2ν , respectively. These qualitative dependences were observed in previous two-pulse studies³⁰ and were predicted in Eqs. (9) and (10) from Section 2 (note that average optical power is proportional to irradiance). To estimate the optical power at the sample, we monitored a small reflection from one of the prisms after attenuation. We calibrated the detected power with spectral filters and an optical powermeter at the position of the sample, but the spectral portions of the light that actually contributed to the QIC signal were not determined for these measurements.

The measured results are clearly consistent with the predicted power dependences from Section 2. Such simple dependences are possible only if the MSM gap resistance remains much greater than the load resistance so that optically induced resistance change can be neglected. The power-dependence measurements strongly support the claim that the ϕ_{CE} sensitivity is due to QIC. The largest signal that we measured throughout all our studies corresponded to a current of 490 pA.

B. Temporal Overlap

We next measured the dependence of the QIC signal on time delay t_d between the two colors at the sample. To do this we monitored the lock-in voltage while scanning one of the two retroreflection mirrors (shown in Fig. 3) with a motorized stage. Figure 5 shows the measured signal as a function of time delay. Each data point represents an average of five measured QIC signal amplitudes. The solid curve represents low-pass fast-Fourier-transform filtering of the measured data.

The QIC signal displays a temporal width of 72 fs. This information is useful for practical purposes when searching for the QIC signal, but it also allows us to estimate the temporal durations of the contributing spectral portions of the pulse. If, for simplicity, we assume identical Gaussian temporal pulse profiles for the two colors, Eq. (5) can be used to verify that a field full width at half-maximum of ~ 60 fs will produce the measured width of $\eta_T(t_d)$. The field widths yield a current pulse excitation of ~ 35 fs for $t_d = 0$ and provide a basis for our assump-

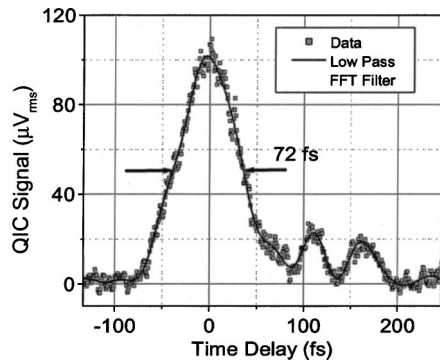


Fig. 5. QIC signal amplitude as a function of the time delay between the two-pulse components near frequencies ν and 2ν . The solid curve represents the low-pass-filtered version of the measured data. FFT, fast Fourier transform.

tion in Section 2 that the pulse width is short compared to the current decay time (~ 200 fs). Also, by using the field width to calculate the Fourier transform-limited spectral width of the pulse spectral regions, we can infer that the contributing spectrum is likely less than 8 nm for the 2ν portion. This result suggests that chirp could limit that portion of the available (~ 25 -nm) spectral wings that is used to generate the QIC signal.

Of related interest are the ripples to the right of the main peak in Fig. 5. Such behavior is typically a signature of third-order dispersion in cross correlation.⁴¹ The inferred spectral width and the ripple both suggest that increased signal strength could be possible with improved dispersion compensation after optimization of the length of microstructure fiber, the prism separation, and the prism insertion shown in Fig. 3.

C. Electrical Characterization of the Source

Because the load impedance of our preamplifier (~ 100 k Ω) was significantly smaller than the MSM shunt resistance during illumination (~ 1 M Ω), we investigated our suspicion that the QIC signal could best be modeled as a constant current source rather than a constant voltage source. We decreased the input load resistance of the voltage preamplifier directly after the QIC sample and monitored the QIC amplitude under the condition $2\pi f_0 RC \ll 1$. For an ideal voltage source, the voltage across the load resistor should remain constant; for an ideal current source, the current should remain constant through the load resistor. In the latter case, the voltage should change in direct proportion to the change in load resistance. Figure 6 shows the measured relative signal amplitude as a function of the load impedance relative to 89 k Ω . The solid line represents the unity slope (direct linear proportionality). The data show direct proportionality between the measured voltage and the load resistance, indicating that the QIC signal behaves like a constant current source for loads below ~ 100 k Ω .

D. Detection Bandwidth

With increased signal amplitude, we could eventually be able to use the QIC signal to stabilize, rather than just measure, f_0 of the laser. To test the applicability of the QIC method for this purpose, we measured the detection bandwidth. We adjusted the reference frequency to

which f_0 was stabilized, monitored changes in the QIC signal peak power on a rf spectrum analyzer, and used a voltage amplifier (gain of 53) following the QIC sample. The results are shown as squares in Fig. 7. The solid curve in Fig. 7 represents the prediction from Eq. (10) by use of the measured values of $R = 89$ k Ω and $C = 74$ pF. Experimental agreement with the simple theory is clear, with both frequency dependences showing a -3 -dB corner at 25 kHz. The MSM structure contributed only a small amount to both R ($R_{\text{MSM}} = 800$ k Ω illuminated) and C ($C_{\text{MSM}} = 1$ – 2 pF, measured without illumination) in this configuration. The largest contributions came from the input impedance of the voltage amplifier and the capacitance of a shielded connecting cable. By decreasing the load resistance into the voltage amplifier, we were able to extend the detection bandwidth to higher frequencies at the expense of signal gain (not shown).

The large shunt resistance allowed us to improve the signal detection bandwidth through transimpedance amplification. The measured QIC signal as a function of stabilization frequency with a transimpedance preamplifier is also shown in Fig. 7. With a transimpedance gain of 10^6 V/A (1-M Ω feedback resistor), we obtained an output voltage of $\sim 1/5$ of that by using the voltage amplifier, as expected, but we increased the bandwidth to 830 kHz and slightly improved the signal-to-noise ratio. The

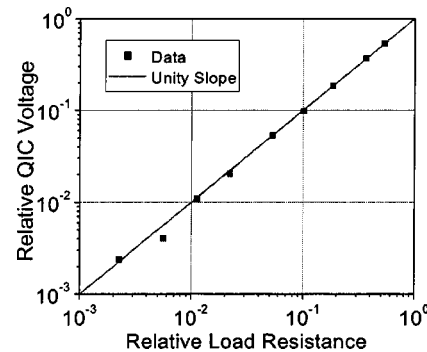


Fig. 6. Relative QIC signal voltage as a function of the load resistance relative to 89 k Ω . The solid line represents the unity slope that is expected from an ideal current source.

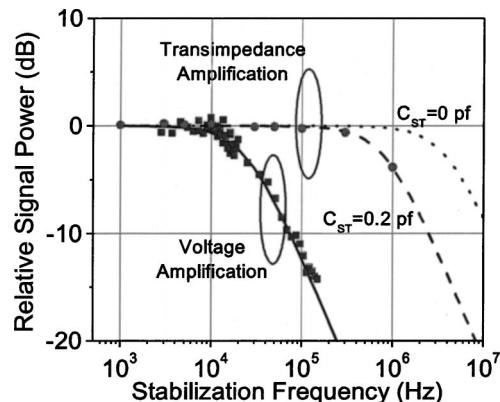


Fig. 7. QIC signal power as a function of the stabilized carrier-envelope offset frequency. The squares (circles) represent data taken with a voltage (transimpedance) amplifier following the QIC sample. The curves represent the predicted behavior from Section 2. C_{ST} , stray capacitance.

dotted curve in Fig. 7 shows the predicted behavior of the signal with the transimpedance amplifier. We attribute the discrepancy between this curve and the measured data to small stray capacitance in parallel with the large feedback resistor of the amplifier. The dashed curve in Fig. 7 shows the predicted behavior when we include a stray capacitance of just 0.2 pF. We anticipate that improved amplifier design will increase the detection bandwidth, but the measured bandwidth is already sufficient for f_0 stabilization.

Transimpedance amplification could also enable the measurement of QIC signals by use of materials with longer carrier lifetimes, such as intrinsic gallium arsenide. In the past, researchers used materials grown at low temperatures, which results in short lifetimes, to ensure that the load impedance of the measurement device remained well below R_{MSM} during illumination. However, our estimates indicate that R_{MSM} for intrinsic GaAs can remain above the input resistance of a transimpedance amplifier if properly designed. This finding could lead to the exploration of QIC in materials that cannot be grown at low temperatures.

E. Additional Observations

By translating the sample through a beam focus, we also measured the nearly 180° phase shift in the QIC signal that is due to the Gouy effect.⁴² The overall magnitude of the phase shift was consistent for all the measurements; however the symmetry of the shift relative to the minimum waist position and the rate of the shift with axial position were not simple and deviated significantly from the Gouy theory. We plan to publish thorough investigations of the Gouy effect in this system in a future publication.

5. CONCLUSIONS

We have investigated the sensitivity of injected photocurrents in low-temperature-grown GaAs to the carrier-envelope phase of ultrashort laser pulses. The observed optical power dependences of the signal were consistent with quantum interference between one- and two-photon absorption. A temporal overlap width of 72 fs suggested that less than 8 nm of spectrum at 2ν contributes to the measured signal. After identifying the signal as a current source for loads under ~ 100 k Ω , we improved the detection bandwidth from 25 to 830 kHz through transimpedance amplification. The low input impedance of such amplifiers could enable the observation of QIC of injected photocurrents in materials with longer carrier lifetimes.

ACKNOWLEDGMENTS

The authors gratefully acknowledge Rich Mirin and Amy VanEngen-Spivey for providing the LT-GaAs samples with lithographic strip lines and Martin Griebel for the useful suggestions and discussions. This research is supported by the National Institute of Standards and Technology, the Office of Naval Research, and the Defense Advanced Research Projects Agency. P. A. Roos (roos@jila.colorado.edu) is supported by the National Academy of Sciences/National Research Council postdoc-

toral fellowship program. S. T. Cundiff is a staff member in the Quantum Physics Division of the National Institute of Standards and Technology. T. M. Fortier's current address is Time and Frequency Division, National Institute of Standards and Technology, 325 Broadway, Boulder, Colorado 80305-3328.

REFERENCES

1. S. T. Cundiff, "Phase stabilization of ultrashort optical pulses," *J. Phys. D* **35**, R43–R59 (2002).
2. L. Xu, Ch. Spielmann, A. Poppe, T. Brabec, F. Krausz, and T. W. Hänsch, "Route to phase control of ultrashort light pulses," *Opt. Lett.* **21**, 2008–2010 (1996).
3. D. J. Jones, S. A. Diddams, J. K. Ranka, A. Stentz, R. S. Windeler, J. L. Hall, and S. T. Cundiff, "Carrier-envelope phase control of femtosecond mode-locked lasers and direct optical frequency synthesis," *Science* **288**, 635–639 (2000).
4. A. Apolonski, A. Poppe, G. Tempea, C. Spielmann, T. Udem, R. Holzwarth, T. W. Hänsch, and F. Krausz, "Controlling the phase evolution of few-cycle light pulses," *Phys. Rev. Lett.* **85**, 740–743 (2000).
5. H. R. Telle, G. Steinmeyer, A. E. Dunlop, J. Stenger, D. H. Sutter, and U. Keller, "Carrier-envelope offset phase control: a novel concept for absolute optical frequency measurement and ultrashort pulse generation," *Appl. Phys. B: Lasers Opt.* **69**, 327–332 (1999).
6. R. Ell, U. Morgner, F. X. Kärtner, J. G. Fujimoto, E. P. Ippen, V. Scheuer, G. Angelow, T. Tschudi, M. J. Lederer, A. Boiko, and B. Luther-Davies, "Generation of 5-fs pulses and octave-spanning spectra directly from a Ti:sapphire laser," *Opt. Lett.* **26**, 373–375 (2001).
7. T. M. Fortier, D. J. Jones, and S. T. Cundiff, "Phase stabilization of an octave-spanning Ti:sapphire laser," *Opt. Lett.* **28**, 2198–2200 (2003).
8. J. K. Ranka, R. S. Windeler, and A. J. Stentz, "Visible continuum generation in air-silica microstructure optical fibers with anomalous dispersion at 800 nm," *Opt. Lett.* **25**, 25–27 (2000).
9. S. A. Diddams, Th. Udem, J. C. Bergquist, E. A. Curtis, R. E. Drullinger, L. Hollberg, W. M. Itano, W. D. Lee, C. W. Oates, K. R. Vogel, and D. J. Wineland, "An optical clock based on a single trapped $^{199}\text{Hg}^+$ ion," *Science* **293**, 825–828 (2001).
10. Th. Udem, J. Reichert, R. Holzwarth, and T. W. Hänsch, "Accurate measurement of large optical frequency differences with a mode-locked laser," *Opt. Lett.* **24**, 881–883 (1999).
11. S. A. Diddams, D. J. Jones, J. Ye, S. T. Cundiff, J. L. Hall, J. K. Ranka, R. S. Windeler, R. Holtzwarth, Th. Udem, and T. W. Hänsch, "Direct link between microwave and optical frequencies with a 300 THz femtosecond laser comb," *Phys. Rev. Lett.* **84**, 5102–5105 (2000).
12. L.-S. Ma, Z. Bi, A. Bartels, L. Robertsson, M. Zucco, R. S. Windeler, G. Wilpers, C. Oates, L. Hollberg, and S. A. Diddams, "Optical frequency synthesis and comparison with uncertainty at the 10^{-19} level," *Science* **303**, 1843–1845 (2004).
13. G. G. Paulus, F. Grasbon, H. Walther, P. Villoresi, M. Nisoli, S. Stagira, E. Priori, and S. De Silvestri, "Absolute-phase phenomena in photoionization with few-cycle laser pulses," *Nature* **414**, 182–184 (2001).
14. G. G. Paulus, F. Lindner, H. Walther, A. Baltuska, E. Goulielmakis, M. Lezius, and F. Krausz, "Measurement of the phase of few-cycle laser pulses," *Phys. Rev. Lett.* **91**, 253004 (2003).
15. F. Lindner, G. G. Paulus, H. Walther, A. Baltuska, E. Goulielmakis, M. Lezius, and F. Krausz, "Gouy phase shift for few-cycle laser pulses," *Phys. Rev. Lett.* **92**, 113001 (2004).
16. A. Baltuska, Th. Udem, M. Uiberacker, M. Hentschel, E. Goulielmakis, Ch. Gohle, R. Holzwarth, V. S. Yakovlev,

- A. Scrinzi, T. W. Hänsch, and F. Krausz, "Attosecond control of electronic processes by intense light fields," *Nature* **421**, 611–615 (2003).
17. M. Nisoli, G. Sansone, S. Stagira, S. De Silvestri, C. Vozzi, M. Pascolini, L. Poletto, P. Villoresi, and G. Tondello, "Effects of carrier-envelope phase differences of few-optical-cycle light pulses in single-shot high-order-harmonic spectra," *Phys. Rev. Lett.* **91**, 213905 (2003).
 18. A. Apolonski, P. Dombi, G. G. Paulus, M. Kakehata, R. Holzwarth, Th. Udem, Ch. Lemell, K. Torizuka, J. Burgdörfer, T. W. Hänsch, and F. Krausz, "Observation of light-phase-sensitive photoemission from a metal," *Phys. Rev. Lett.* **92**, 073902 (2004).
 19. P. Dombi, A. Apolonski, Ch. Lemell, G. G. Paulus, M. Kakehata, R. Holzwarth, Th. Udem, K. Torizuka, J. Burgdörfer, T. W. Hänsch, and F. Krausz, "Direct measurement and analysis of the carrier-envelope phase in light pulses approaching the single-cycle regime," *New J. Phys.* **6**, 1–17 (2004).
 20. O. D. Mücke, T. Tritschler, M. Wegener, U. Morgner, and F. X. Kärtner, "Signatures of carrier-wave Rabi flopping in GaAs," *Phys. Rev. Lett.* **87**, 057401 (2001).
 21. O. D. Mücke, T. Tritschler, M. Wegener, U. Morgner, and F. X. Kärtner, "Role of the carrier-envelope offset phase of few-cycle pulses in nonperturbative resonant nonlinear optics," *Phys. Rev. Lett.* **89**, 127401 (2002).
 22. Q. T. Vu, H. Haug, O. D. Mücke, T. Tritschler, M. Wegener, G. Khitrova, and H. M. Gibbs, "Light-induced gaps in semiconductor band-to-band transitions," *Phys. Rev. Lett.* **92**, 217403 (2004).
 23. O. D. Mücke, T. Tritschler, M. Wegener, U. Morgner, F. X. Kärtner, G. Khitrova, and H. M. Gibbs, "Carrier-wave Rabi flopping: role of the carrier-envelope phase," *Opt. Lett.* **29**, 2160–2162 (2004).
 24. O. D. Mücke, T. Tritschler, M. Wegener, U. Morgner, and F. X. Kärtner, "Determining the carrier-envelope offset frequency of 5-fs pulses with extreme nonlinear optics in ZnO," *Opt. Lett.* **27**, 2127–2129 (2002).
 25. M. Wegener, Institut für Angewandte Physik, Universität Karlsruhe (TH), Wolfgang-Gaede-Strasse 1, 76131 Karlsruhe, Germany (personal communication, 2004).
 26. R. Atanasov, A. Haché, J. L. P. Hughes, H. M. van Driel, and J. E. Sipe, "Coherent control of photocurrent generation in bulk semiconductors," *Phys. Rev. Lett.* **76**, 1703–1706 (1996).
 27. A. Haché, Y. Kostoulas, R. Atanasov, J. L. P. Hughes, J. E. Sipe, and H. M. van Driel, "Observation of coherently controlled photocurrent in unbiased, bulk GaAs," *Phys. Rev. Lett.* **78**, 306–309 (1997).
 28. A. Haché, J. E. Sipe, and H. M. van Driel, "Quantum interference control of electrical currents in GaAs," *IEEE J. Quantum Electron.* **34**, 1144–1154 (1998).
 29. H. M. van Driel and J. E. Sipe, "Coherent control of photocurrents in semiconductors," in *Ultrafast Phenomena in Semiconductors*, K.-T. Tsen, ed. (Springer, New York, 2001), pp. 261–307 and references therein.
 30. P. A. Roos, Q. Quraishi, S. T. Cundiff, R. D. R. Bhat, and J. E. Sipe, "Characterization of quantum interference control of injected currents in LT-GaAs for carrier-envelope phase measurements," *Opt. Express* **11**, 2081–2090 (2003), <http://www.opticsexpress.org>.
 31. T. M. Fortier, P. A. Roos, D. J. Jones, S. T. Cundiff, R. D. R. Bhat, and J. E. Sipe, "Carrier-envelope phase-controlled quantum interference of injected photocurrents in semiconductors," *Phys. Rev. Lett.* **92**, 147403 (2004).
 32. R. D. R. Bhat and J. E. Sipe, "Optically injected spin currents in semiconductors," *Phys. Rev. Lett.* **85**, 5432–5435 (2000).
 33. H. M. van Driel, Y. Kerachian, P. Nemeč, and A. L. Smirl, "Quantum interference injection and control of spin-polarized transient current gratings in GaAs," *Semicond. Sci. Technol.* **19**, S223–S225 (2004), and references therein.
 34. E. Dupont, P. B. Corkum, H. C. Liu, M. Buchanan, and Z. R. Wasilewski, "Phase-controlled currents in semiconductors," *Phys. Rev. Lett.* **74**, 3596–3599 (1995).
 35. Y.-Y. Yin, C. Chen, D. S. Elliott, and A. V. Smith, "Asymmetric photoelectron angular distributions from interfering photoionization processes," *Phys. Rev. Lett.* **69**, 2353–2356 (1992).
 36. D. Z. Anderson, N. B. Baranova, K. Greene, and B. Y. Zel'dovich, "Interference of one- and two-photon processes in the ionization of atoms and molecules," *Sov. Phys. JETP* **75**, 210–214 (1992).
 37. Q. Wang and A. F. Starace, "Short-pulse detachment of H⁻ in the presence of a static electric field," *Phys. Rev. A* **48**, R1741–R1744 (1993).
 38. B. Sheehy, B. Walker, and L. F. DiMauro, "Phase control in the two-color photodissociation of HD⁺," *Phys. Rev. Lett.* **74**, 4799–4802 (1995).
 39. M. Abramowitz and I. A. Stegun, eds., *Handbook of Mathematical Functions with Formulas, Graphs, and Mathematical Tables* (U.S. Department of Commerce, Washington, D.C., 1972), p. 1020.
 40. J. M. Fraser, A. Haché, A. I. Shkrebti, J. E. Sipe, and H. M. van Driel, "Three color coherent generation and control of current in low-temperature-grown GaAs," *Appl. Phys. Lett.* **74**, 2014–2016 (1999).
 41. C.-C. Chang, A. M. Weiner, A. M. Vengsarkar, and D. W. Peckham, "Broadband fiber dispersion compensation for sub-100-fs pulses with a compression ratio of 300," *Opt. Lett.* **21**, 1141–1143 (1996).
 42. A. E. Siegman, *Lasers* (University Science, Mill Valley, Calif., 1986), Chap. 17.4.